ISSN 2616-5767 Vol.7, Issue 3: 17-28, DOI: 10.25236/AJETS.2024.070304

Sound Source Analysis of Blade Aerodynamic Noise of Megawatt Wind Turbine Based on Vortex Sound Theory

He Ruirong[1,a], Liu Houcai[1], Kang Huimin[1,b,*], Zhang Xuewen[2], Xi Jiale[1], Shen Xiangjun[1]

[1]*School of Mechanical Engineering, Hunan University of Science and Technology, Xiangtan, China*
[2]*National Key Laboratory of Offshore Wind Power Equipment and Efficient Utilization of Wind Energy, Xiangtan, China*
[a]*qwe578204617@163.com,* [b]*1030096@hnust.edu.cn*
[*]*Corresponding author*

Abstract: *Based on the analysis method of vortex sound theory, the mechanism of turbine blade aerodynamic noise generation is studied. In this paper, modeling and grid division of wind turbine blades and flow field areas are first carried out, and the directivity of wind turbine aerodynamic noise is analyzed by CFD (computational fluid dynamics) numerical simulation calculation. Through test verification, it is concluded that wind turbine aerodynamic noise is a dipole characteristic, and the accuracy of numerical simulation is verified. Then, the distribution of flow field and sound field calculated by numerical simulation are analyzed and compared, and the main causes of wind turbine blade aerodynamic noise are studied. The results show that the aerodynamic noise sources of wind turbine blades are mainly distributed in 65%~95% span of the blade spanwise direction. At the same time, the sound source of wind turbine blade aerodynamic noise is mainly caused by vortex movement caused by fluid movement, and the distribution law of vortex movement in the range of 65%~95% of blade span is very consistent with the distribution law of blade aerodynamic noise.*

Keywords: *Aerodynamic noise, Wind turbine blade, Vortex sound theory, Vortex motion*

1. Introduction

Wind energy is being promoted as a sustainable and clean energy source by governments all over the world. The influence of wind turbine noise on the environment has steadily become an important topic of increasing concern in recent years, owing to the large-scale design of wind-driven generators as well as the mass-scale construction of wind farms. Wind turbine noise is classified as mechanical noise or aerodynamic noise, with aerodynamic noise being more noticeable than mechanical noise [1].

Research on aerodynamic noise, both domestic and international, dates back to the 1950s. Powell [2] proposed the vortex sound theory for the first time. He pointed out that when fluid flows at a low speed, sound can only be generated in the vortex region, which provided an important theoretical basis for the study of underwater noise and aerodynamic noise. Subsequently, Howe [3-4] extended the vortex sound theory on the basis of vorticity and vortex force distribution in unsteady flow, and believed that the radiation of sound waves was closely related to the structure and size of vortices in fluid, further improving Powell's vortex sound theory. Based on this, Violato D.[5] et al. investigated jet vortex acoustics at low Mach number conditions using time-resolved planar and laminar PIVs, and found significant acoustic radiation, particularly in the vortex instability and vortex rupture orientations. S.K. Tang [6] further argued that vortex movement is one of the leading elements of pneumatic noise source, which is almost the only source in a flow field with a small Mach number. Zheng et al. [7] discovered that cylinder noise is caused by unsteady vortex motion during vortex shedding, as observed through time-resolved particle image velocity measurement experiments. The intensity of vortex shedding is correlated with the size of aerodynamic noise. Ouyang [8] et al. used PIV and CFD for a comparative study of the air-fluid field of a low-speed axial fan and pointed out that the aerodynamic noise principally occasions from the stretching and rupture of vortices in the airflow field under low-speed isentropic flow conditions, and the main aerodynamic sound sources' distribution and their relative intensities were identified with adopting vortex sound theory combined with the means of CFD numerical simulation. Zhang [9] et al. compared

ISSN 2616-5767 Vol.7, Issue 3: 17-28, DOI: 10.25236/AJETS.2024.070304

the NACA0012 airfoil's aerodynamic noise by numerical simulation adopting the vortex sound theory and the FW-H acoustic analog theory. The results displayed that both methods could precisely predict the noise aroused by an unsteady fluid field. Through a mix of simulation and experimentation, Qiaorui Si et al. [10] looked into the linking process between the DP fluid field and the sound field. They discovered that turbulent pulsation and eddy current, two no steady flows in the fluid field, were strongly associated with the production of fluid noise.

There have been more in-depth studies on the generation of fluid noise by using the vortex sound theory, but there are no relevant studies on the generation of wind turbine aerodynamic noise by using the vortex sound theory. In this paper, a 2.5MW wind turbine blade is taken as the research object, modeling and numerical simulation are completed through the numerical simulation software ANSYS Fluent, and the aerodynamic noise sound source of wind turbine blade is studied by using the analysis method of vortex sound theory. The distribution of aerodynamic noise source and the motion of fluid in the flow field are analyzed in order to study the cause of aerodynamic noise source of wind turbine. This study has a certain reference value for further analysis of wind turbine blade aerodynamic noise reduction mechanism.

2. Theoretical Analysis of Aerodynamic Noise of Blades

2.1. Theoretical Equation of Vortex Sound under Rotating Conditions of Wind Turbine

To reveal the correlation of fluid vorticity with the generation mechanism of aerodynamic noise, according to the vortex sound theory, it can acquire the equation as [2]:

$$\frac{\partial^2 p}{\partial t^2}-c_0^2\nabla^2 p=\nabla\cdot\left[\rho_0\left(\vec{\omega}\times\vec{v}\right)+\rho_0\nabla\frac{\vec{v}^2}{2}-\vec{v}\frac{\partial\rho}{\partial t}-\frac{\vec{v}^2}{2}\nabla p+\nabla\left(p-\rho c_0^2\right)\right] \tag{1}$$

Where, ∇ is the Hamiltonian operator, c_0 is the sound velocity. ρ is air fluid density, t is time, $\vec{v}$ is velocity, $\vec{\omega}$ is vorticity, p is air fluid pressure.

In the actual operation of wind turbines, the speed of fluid in the flow field is much less than the speed of sound c_0. Combined with the Mach number formula $M_a = v/c_0$ and its definition, it can be seen that the flow field of wind turbines during operation belongs to low Mach number flow field [20]. Because in adiabatic isentropic fluid motion with low Mach number, the vorticity equation can ignore the high-value term, so equation (1) can be simplified as [11]:

$$\frac{1}{c_0^2}\frac{\partial^2 p_i}{\partial t^2}-\nabla^2 p_i=\nabla\cdot\left[\rho_0\left(\vec{\omega}\times\vec{v}\right)+\rho_0\nabla\frac{\vec{v}^2}{2}\right] \tag{2}$$

In the above equation, the differential equation on the left is the wave equation of sound pressure, which represents the acoustic properties of the sound wave propagation process. The right-hand of the equal sign in the equation (2) is the sound source, representing the source of the radiated sound wave. From the right of the source term can be acquired that the size of the sound source is attributed to the fluid motion of vortex stretching distortion $[\nabla\cdot(\rho_0(\vec{\omega}\times\vec{v}))]$ and the fluid kinetic energy $[\nabla^2(\rho_0\vec{v}/2)]$.

2.2. Airflow Vorticity Control Equation

The aerodynamic noise generated by wind turbine blades is closely related to the vortex motion. In order to accurately analyze the vortex motion, the vorticity characteristics in the flow field must be deeply analyzed. With constant fluid density, the governing equation of airflow vorticity is as follows [12]:

$$\frac{D\vec{\omega}}{Dt}=\left(\vec{\omega}\cdot\nabla\right)\vec{v}-\vec{\omega}\left(\nabla\cdot\vec{v}\right)+\frac{1}{\rho^2}\nabla\rho\times\nabla p+\nabla\times\vec{f}+\frac{\eta\nabla^2\vec{\omega}}{\rho} \tag{3}$$

Where, η is the viscosity coefficient, and f is the volume force of the fluid.

Because the fluid analyses in this research is an air-fluid when the wind power generator blade is rotating and its density is constant, that is, the influences of volume change $\vec{\omega}(\nabla\cdot\vec{v})$, positive pressure$(\nabla\rho\times\nabla p)$ and volume force $\left(\nabla\times\vec{f}\right)$ can be ignored, equation (3) can be further simplified as follows:

ISSN 2616-5767 Vol.7, Issue 3: 17-28, DOI: 10.25236/AJETS.2024.070304

$$\frac{D\vec{\omega}}{Dt} = (\vec{\omega}\cdot\nabla)\vec{v} + \frac{\eta\nabla^2\vec{\omega}}{\rho} \tag{4}$$

The changing rate of vorticity with the flow of fluid is represented by the left-hand of the equal sign in the equation above. The change in the direction and magnitude of vorticity brought on by a change in velocity is represented by the first component on the right-hand side of the eq. (4) $[(\vec{\omega}\cdot\nabla)\vec{v}_l]$ (gradient of velocity). The fluid's viscous force causes a change in vorticity diffusion, which is represented by the second term $(\eta\nabla^2\vec{\omega}/\rho)$.

3. Construction of Numerical Simulation Model of Wind Turbine Blade Aerodynamic Noise and Noise Directivity Verification

3.1. Geometric Models and Meshing

This paper takes the blades of 2.5MW wind turbine XE122-2500 as the research object, and its parameters are shown in Table 1. The blade length R of the wind turbine is 59.5m.

Table 1: Main geometric parameters of the wind turbines.

Parameter	value
Rated power	2500kw
Applicable wind zone	IEC S
Rate speed	12.8r/min
Number of blades	3
Length of blades	59.5m
Diameter of impeller	122m
Tower height	87.5m
Wind wheel inclination angle	5°

In order to improve the convergence of numerical simulation calculation, the structure of the model is simplified, ignoring the wheel hub and tower. The calculation area of the wind turbine flow field model is divided into the rotating near-flow field area near the blade and the outer flow field area. The spatial division design of the flow field calculation area is shown in Figure 1.

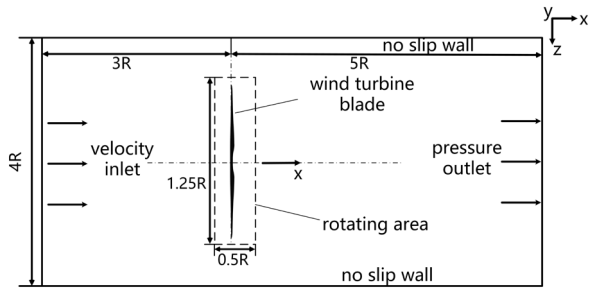

Figure 1: Spatial division of fluid field calculation area.

The mesh of the simulation calculation area adopts segmented processing, including the blade surface mesh, the near flow field rotation area mesh, and the outer laminar flow field area mesh. In order to generate high-quality boundary layer mesh on the blade surface, structured mesh is used for blade surface mesh, as shown in Figure 2. Since the numerical simulation is solved using the finite element software ANSYS Fluent, the overall space mesh is specified as follows: The outer flow field area adopts a relatively large hexahedral structure mesh to save the number of grids; Considering that the calculation of the rotation region of the near-flow field is complicated, a finer unstructured mesh is used; As k-omega SST turbulence model is adopted in this paper, y+ value should be controlled within 0~10 [13], and the growth rate of boundary layer should be set at 1.15. The overall mesh situation of the numerical simulation calculation area is shown in Figure 3.

ISSN 2616-5767 Vol.7, Issue 3: 17-28, DOI: 10.25236/AJETS.2024.070304

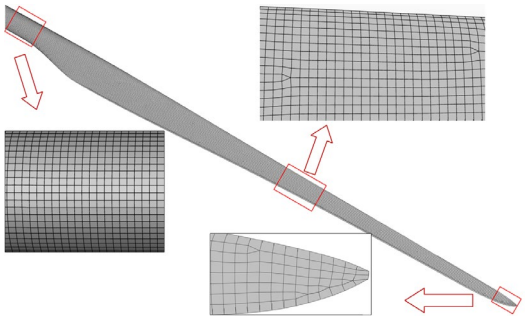

Figure 2: Blade model and blade surface mesh.

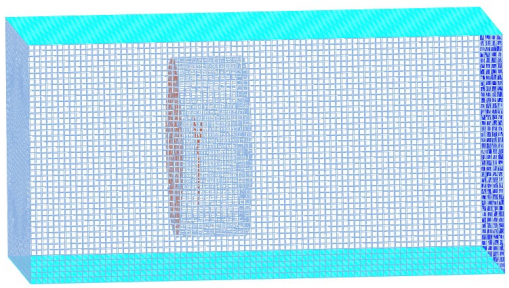

Figure 3: The mesh of the calculation area.

In order to reduce the error of simulation results as much as possible, a total of 4 different mesh quantities were set for grid independence verification, as shown in Table 2. When the number of meshes is greater than 5.42 million, the difference of mass flow rate between import and export remains almost constant with the increase of the number of meshes, and the relative error of the difference of flow rate between import and export is less than 2%. Relevant studies show [14] that when the relative error of the difference between the inlet and outlet flow is less than 2%, the influence of the number of grids can be ignored. Therefore, on the basis of ensuring the accuracy and cycle of simulation calculation, the second group mesh is selected for simulation.

Table 2: Numerical simulation mesh number independence verification.

Number	Mesh quantity	Mass flow rate difference
1	4.57×10^{6}	2.26×10^{-3}
2	5.42×10^{6}	3.12×10^{-4}
3	6.33×10^{6}	3.08×10^{-4}
4	7.15×10^{6}	3.03×10^{-4}

3.2. Setting of Boundary Conditions

According to the practical situation of wind power generator operation and the requirements of ANSYS Fluent, the boundary conditions of the calculation region are defined as follows: The inlet boundary of the flow field is set as the inlet boundary condition of the velocity, the flow rate is 12m/s, and the fluid flows horizontally through the calculation domain along the X-axis direction; The outlet boundary is defined as pressure outlet. In addition, the pressure is a standard atmospheric pressure value; The blade and the surrounding outer walls are designed as symmetry surfaces, and the blade's deformation is not considered. The flowing medium is air, and MRF method is used in the near flow field rotation region. The blade surface rotates along with the near-flow field rotation region. At the same time, since the rotational speed of the turbine impeller generally runs in the range of 6.5 to 8 r/min, the rotational speed n of the rotating area is set to 7r/min. In addition, the rotational speed n was set to 5r/min as the reference control group, so that comparative analysis could be performed after calculation.

3.3. Validation of Numerical Models

3.3.1. Directional Analysis of Sound Field

When a sound source radiates sound waves outward in a free field, the sound pressure level shows an uneven property with different directions, which is called the directivity of the sound source. In order to verify the rationality of the numerical calculation method, the sound source directivity of the sound field is analyzed and compared with the experiment. The specific setting of noise directivity monitoring points is shown in Figure 4. Taking the XOZ plane as the reference plane, a total of 36 sound receiving points are set on a 1.25R radius circle with the center of the impeller as the origin plane, which is parallel to the reference plane and 1.25R apart.

ISSN 2616-5767 Vol.7, Issue 3: 17-28, DOI: 10.25236/AJETS.2024.070304

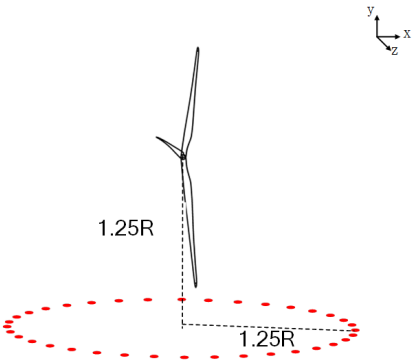

Figure 4: Noise directivity monitoring points are set.

Figure 5 shows the noise directivity diagram of wind turbine aerodynamic noise. The directivity distribution of the sound pressure level of the wind turbine aerodynamic noise is similar at two rotational speeds, and the sound pressure level of the noise at 0° and 180° is the largest, while the sound pressure level of the noise at 90° and 270° is the smallest. For example, when the impeller speed is 5 r/min, the sound pressure levels at 0°, 180°, 90° and 270° are 76.9dB, 76.8dB, 66.3dB and 69.9dB, respectively. When the impeller speed is 7 r/min, the sound pressure level values are 93.3dB, 93.1dB, 82.1dB and 85.2dB, respectively, and the sound pressure level values of 5 r/min and 7 r/min differ by about 13-16dB on the whole. From the overall appearance in the figure, the directional distribution of wind turbine aerodynamic noise presents an "∞" type distribution of drums at both ends and concave at both sides of the middle, which belongs to the dipole sound source.

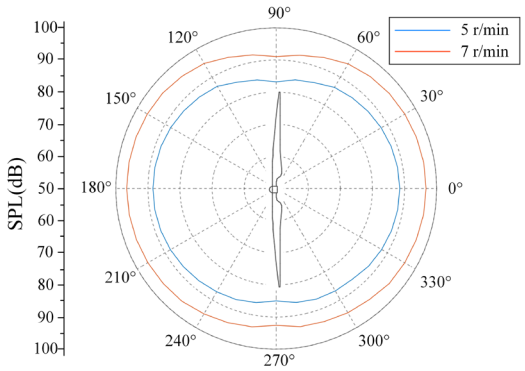

Figure 5: Directional diagram of wind turbine aerodynamic noise.

3.3.2. Experimental Verification of Sound Field Directivity

The test site is in the booster station of Bao Zhongshan Wind Farm, Xiangxiang City, Hunan Province. The 8# unit selected for the test has a power of 2.5MW, and its parameters are consistent with those in Table 1. The wind turbine is shown in Figure 6. The sound pressure level is monitored by a VICTOR824 noise analyzer with a measuring range of 30~130dB.

Figure 6: 2.5MW wind turbine.

Figure 7: Wind turbine host computer monitoring system.

The monitoring of the speed of the impeller can be carried out in real time through the monitoring

ISSN 2616-5767 Vol.7, Issue 3: 17-28, DOI: 10.25236/AJETS.2024.070304

system of the upper computer, as shown in Figure 7. According to the Settings of the above simulation, it is necessary to ensure that the speed of the impeller is within the range of 7.0±0.2r/min during the test measurement. In accordance with the test standards of GB/T 22156-2015 "Wind Turbine Noise Measurement Method", the distribution of noise measurement points in the noise test is consistent with the noise monitoring points set by the simulation. Each noise measurement point is measured three times, and the test measurement results are shown in Figure 8.

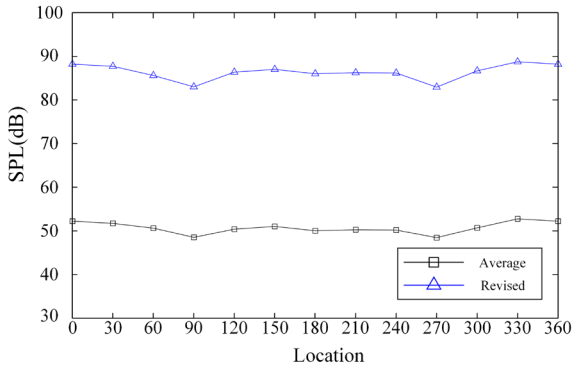

Figure 8: The measured noise value and the corrected value.

In Figure 8, the black curve with positive direction is the average value of 3 measurements at each measurement point. The blue curve with triangle is the corrected noise value based on the measured value of the test, adding the sound attenuation factor. This is due to the fact that sound waves are affected by factors such as medium absorption, propagation distance, and other factors that cause sound pressure to gradually weaken[15]. But, when calculating the sound field for the simulation, the fluid motion factor is the only factor taken into account, with the sound's attenuation characteristics being disregarded.

Figure 9 shows the noise directivity diagram after the correction of test measurement and numerical simulation calculation. As can be seen from the figure, the numerical simulation results of aerodynamic noise directivity are basically similar to the modified experimental measurement results, and on the whole, they are also consistent with the dipole directivity distribution characteristics of the concave (" ∞ ") middle sides of the front and back ends of the drum. The noise pressure level at 90° and 270° is smaller, which is 81.3dB and 82.9dB respectively. The sound pressure level of the noise at 0° and 180° is larger, which is 86.9dB and 86.8dB respectively. The difference between the noise value obtained by the numerical simulation and the modified test measurement value is 5~6dB in general, and the maximum error is 8%, which is good agreement, and verifies the accuracy of the numerical model. It increases the reliability of the analysis of the simulation results.

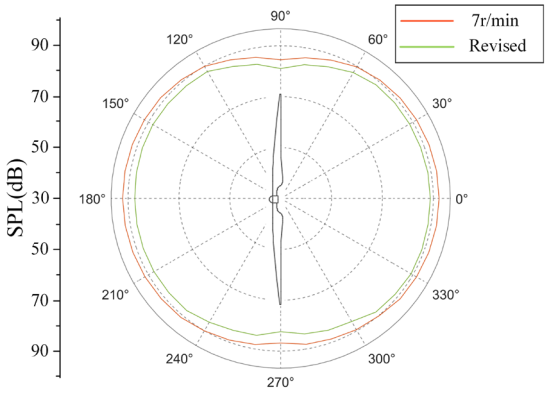

Figure 9: Comparison of noise directivity between numerical simulation and experimental modification.

4. Analysis of Numerical Simulation Results of Aerodynamic Noise

4.1. Distribution Analysis of Blade Aerodynamic Noise Source

Through numerical simulation and calculation of sound field, the aerodynamic noise distribution of

ISSN 2616-5767 Vol.7, Issue 3: 17-28, DOI: 10.25236/AJETS.2024.070304

wind turbine blades is shown in Figure 10. In order to obtain the sound pressure level (SPL) values of noise sources at each position on the blade more intuitively from the cloud map of aerodynamic noise source distribution in Figure 10, cloud view values were used to filter the positions of the blade, extract the maximum sound pressure level values of noise sources at each span position, and draw a curve to facilitate analysis, as shown in Figure 11.

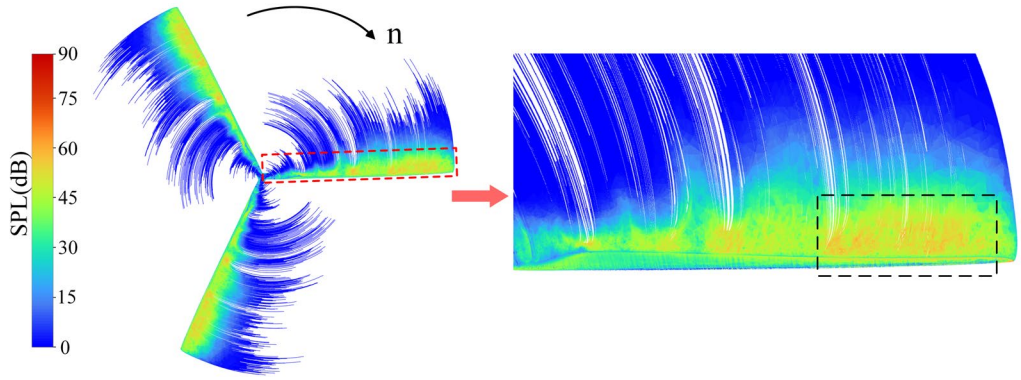

a. n= 5 r/min

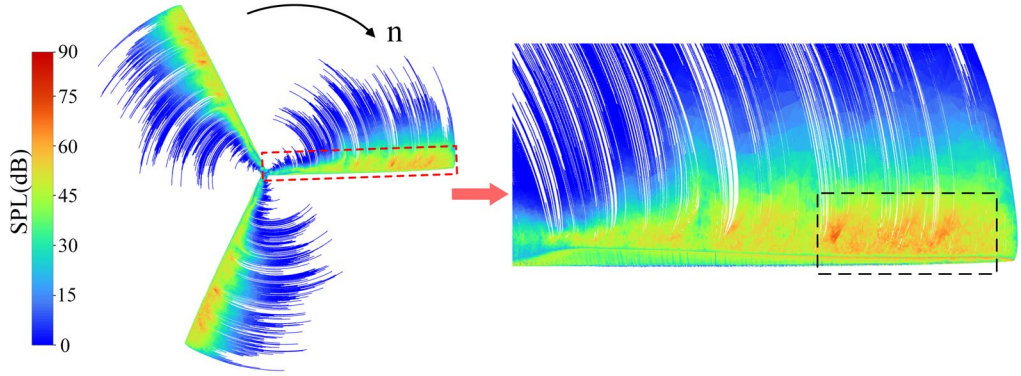

b. n= 7 r/min

Figure 10: Distribution cloud image of sound source of aerodynamic noise of blade at different speed.

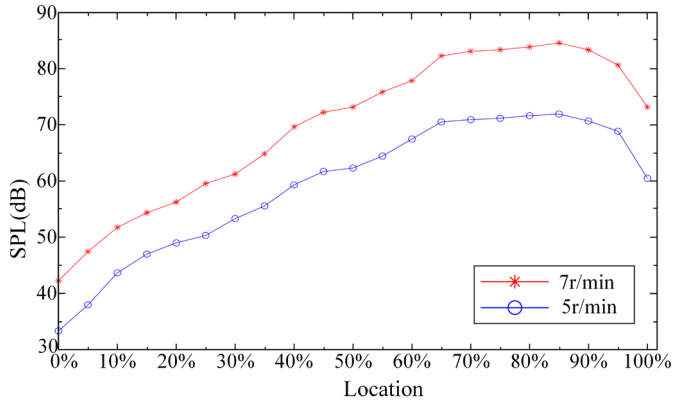

Figure 11: Noise sound pressure level maximum distribution.

As shown in Figure 10 and 11 the distribution rule of the SPL of the blade noise source is similar at both rotational speeds. The more quickly the impeller rotating speed, the higher the acoustic pressure level of the entire noise source of the blade. When the blade is at the span of 0% to 65%, the SPL of the noise source increases gradually. In the 65%-95% span (the area with black dashed lines in Figure 10), the SPL of the noise source reaches the maximum value, which is 71.8dB and 84.5dB respectively, and the value of the SPL fluctuates slightly (the fluctuation is less than 2dB). It shows that the blade noise mainly occurs in this span region. At 95%~100% span, the acoustic pressure level of the noise source decreases significantly, from 68.8dB and 80.6dB to 60.4dB and 73.1dB respectively.

According to the relevant formula of wind turbine noise prediction [16], the noise of the blade at 0% to 95% span segments is induced by the air fluid near the wake (turbulent boundary layer), which belongs

ISSN 2616-5767 Vol.7, Issue 3: 17-28, DOI: 10.25236/AJETS.2024.070304

to the trailing edge noise of the blade. In the 0%~ 65% span, due to the gradual formation of turbulence on the blade surface, the thickness of the boundary layer increases gradually, the corresponding noise pressure level also increases gradually, and the value of SPL increases relatively fast. In the 65%-95% span, the flow on the blade surface reaches the turbulent state, the turbulent boundary layer thickness reaches the maximum, and the value of SPL also reaches the maximum. However, the noise in the 95%-100% span is caused by the air fluid at the tip of the wind-driven generator blade, which belongs to the tip vortex noise, and its acoustic pressure level has a downward trend. It indicates that the trailing edge aerodynamic noise of wind power generator blades is much larger than the tip vortex aerodynamic noise. From the superposition characteristics of sound pressure, it can be acquired that the SPL of the noise source depends on the maximum value of the superposition of sound pressure[17]. Therefore, it can be considered that the 65%~95% span of the blade extension direction is the main sound source area of aerodynamic noise.

4.2. Sound Source Analysis of Blade Aerodynamic Noise

In order to obtain more detailed noise distribution information in the main sound source area of the blade aerodynamic noise, four monitoring cross sections are set in the main noise source area, as shown in Figure 12. The reference plane of the monitoring cross-section is determined by taking the plane XOY, which is perpendicular to the plane XOZ. The monitoring cross section is positioned at 65%, 75%, 85%, and 95% of the blade's spread direction along the positive Z axis, respectively. This allows for a thorough examination of the flow field velocity, fluid kinetic energy, and acoustic pressure level of noise of each cross-section.

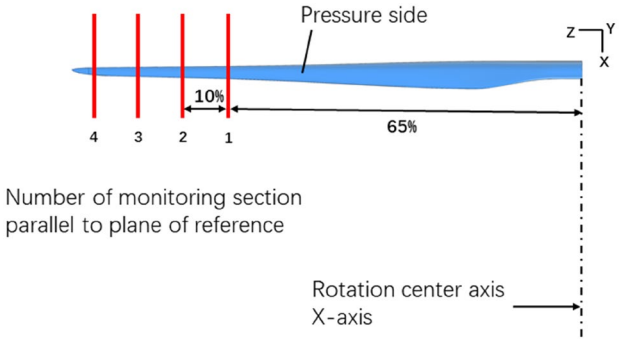

Figure 12: Location of each monitoring section.

4.2.1. Analysis of vortex motion

According to the four monitoring cross sections set in Figure 12, the axial flow velocity distribution cloud image obtained on each monitoring cross section is shown in Figure 13. The dashed black line in the figure is the zero value line. In the area other than the dashed black line, the fluid field velocity value is positive; In the area within the black dashed line, the fluid field velocity value is negative.

As can be seen from Figure 13, both positive and negative flow rates exist on the monitoring cross sections of the four sound sources, indicating the presence of inverse-pressure-separated flow in each region [18]. This inverse-pressure-separated flow phenomenon is a necessary and sufficient condition for the formation of vortices, which will produce vortices in each monitoring section. At the same time, the area of the black dashed line in Figure 13 gradually increases along the blade spread direction. It shows that the motion of the fluid causes the vortex to stretch.

In order to obtain the velocity gradient changes on each monitoring cross section in Figure 13, the maximum positive velocity and maximum negative velocity on each monitoring cross section were extracted from the velocity distribution cloud map in Figure 13 successively, and the difference between them was obtained. The maximum positive and negative velocity values in each section are located at the wake of the blade and the center of the vortex, respectively, and their differences are shown in Table 3.

ISSN 2616-5767 Vol.7, Issue 3: 17-28, DOI: 10.25236/AJETS.2024.070304

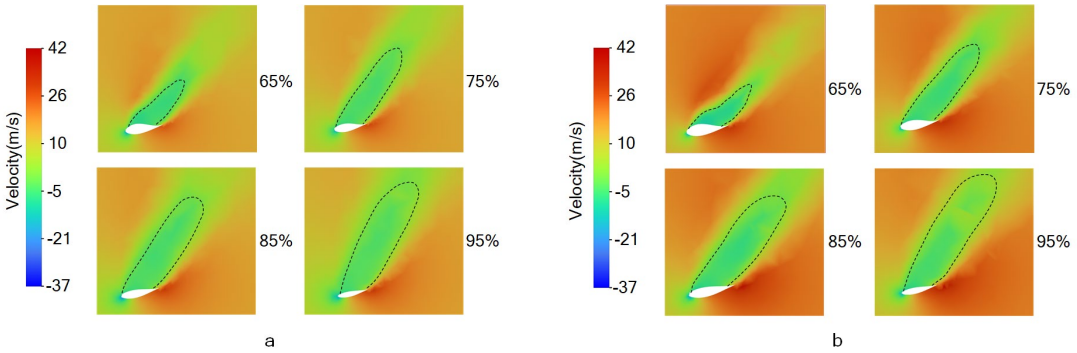

(a. n=5r/min; b. n=7r/min)

Figure 13: Velocity distribution in the direction of the fluid axis on each monitoring cross section.

Table 3: The maximum positive value of the velocity at the wake, the maximum negative value of the velocity in the center of the vortex and its difference on each monitoring cross section (m/s).

n=5r/min				n=7r/min			
Position	Wake	Vortex region	Difference	Position	Wake	Vortex region	Difference
65%	32	-5.2	37.2	65%	40.5	-9.6	50.1
75%	32.5	-5.1	37.6	75%	41.1	-9.2	50.3
85%	32.8	-5.1	37.8	85%	41.6	-9.3	50.9
95%	33.1	-2.2	35.3	95%	41.8	-5.0	46.8

As can be seen from Table 3, the difference between the positive value of the maximum velocity at the wake of the blade and the negative value of the maximum velocity in the vortex region (the velocity gradient) gradually increases in the span of 65%~85%, but the increase is small. For example, when the impeller speed is 5.8r/min, it only increases by 0.6 m/s; When the impeller speed is 7r/min, the increase is 0.8 m/s. However, the velocity gradient within 85%~95% of the span is reduced, and the reduction is large. The reduction is 2.5 m/s when the impeller speed is 5.8 r/min and 4.1 m/s when the impeller speed is 7 r/min. According to equation (4), the vorticity generated by the airflow only increases slightly in 65%~85% of the span. However, within 85%~95% of the span, the vorticity produced by the airflow decreases greatly.

4.2.2. Analysis of Kinetic Energy of Fluid

According to the monitoring cross section set in Figure 12, the distribution cloud image of fluid kinetic energy obtained on each monitoring cross section is shown in Figure 14.

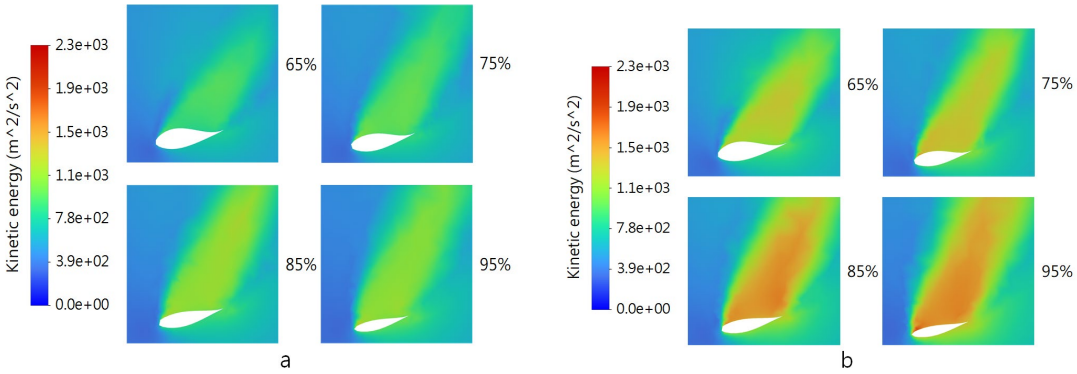

(a. n=5r/min; b. n=7r/min)

Figure 14: Cloud view of fluid kinetic energy distribution on each monitoring cross section.

It can be seen from Figure 14 that the maximum kinetic energy of the fluid on each section is on one side of the pressure surface of the blade, and the greater the rotational speed of the impeller, the greater the kinetic energy of the fluid on the pressure surface. When the impeller is at the same speed, the fluid kinetic energy of the blade in 65%~95% span and its distribution area are increasing along the development direction. The specific fluid kinetic energy values are shown in Table 4.

ISSN 2616-5767 Vol.7, Issue 3: 17-28, DOI: 10.25236/AJETS.2024.070304

Table 4: Numerical simulation grid number independence verification.

Section position	65%	75%	85%	95%
5r/min	772	994	1089	1167
7r/min	1228	1431	1647	1889

4.2.3. Analysis of the Influence of Vortex Motion and Kinetic Energy of Fluid on Aerodynamic Noise of Blades

Figure 15 is the cloud view of noise pressure level distribution on each monitoring section. Meanwhile, in order to more directly reflect the noise generated by noise sources at different speeds and different positions of wind turbine blades, the maximum sound pressure level value at the corresponding position is extracted from the cloud map of noise pressure level distribution on each monitoring section, as shown in Table 5.

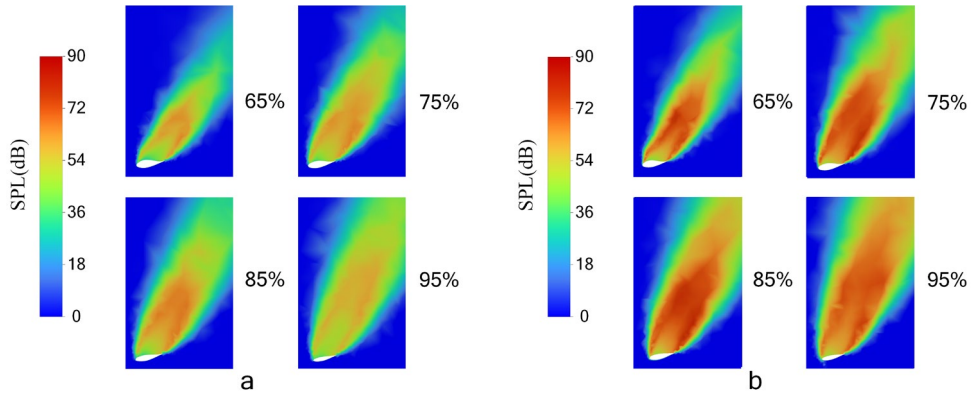

(a. n=5r/min; b. n=7r/min)

Figure 15: Cloud view of noise pressure level distribution on each monitoring cross section.

Table 5: The maximum noise pressure level of each monitoring section.

Section position	65%	75%	85%	95%
5r/min	70.4	71.1	71.8	68.8
7r/min	82.2	83.3	84.5	80.6

As can be seen from Figure 15 and Table 5, at each monitoring cross-section of the same span, when the impeller speed of 5.8r/min, the value of the noise acoustic pressure level is significantly smaller than the value of the noise acoustic pressure level at the impeller speed of 7r/min. The difference between the two noise SPLs is about 12dB, and the noise distribution area of the latter is slightly larger than that of the former. When the impeller is at the same speed, the magnitude of the noise acoustic pressure level and the distribution area has a small increase in the blade 65% ~ 85% of the span; in the 85% ~ 95% of the span, the noise acoustic pressure level has been reduced, but the distribution area has been still increased.

According to Figure 13 and Figure 15, it can be seen that the variation law of the distribution range of the vortex region and the variation law of the velocity gradient between the wake and the vortex region are consistent with the variation law of the distribution range of the noise source and the variation law of the noise pressure level, respectively. For example, the distribution range of the vortex region gradually increases in the 65%-95% span segment, and the distribution range of the noise source also gradually increases in the span segment. The velocity gradient in the vortex region and wake increases first and then decreases in the 65%-95% span, and the sound pressure level of the noise source also increases first and then decreases in the span. Therefore, it is reasonable to think that the distribution law of sound pressure level of wind turbine blade aerodynamic noise source is completely consistent with the distribution law of vortex motion.

However, by comparing Figure 14 and Figure 15, it's not hard to find that the variation rule of the fluid kinetic energy at 65%~95% of the span is inconsistent with the variation rule of the SPL of the pneumatic noise source. Especially on the span of 85%~95%, the magnitude of the blade aerodynamic noise source SPL tends to decrease, while the magnitude of the fluid kinetic energy increases instead of decreasing. Therefore, the hydrodynamic energy is not the main cause of aerodynamic noise of wind

ISSN 2616-5767 Vol.7, Issue 3: 17-28, DOI: 10.25236/AJETS.2024.070304

turbines, which also indicates that the main sound source of aerodynamic noise of wind turbines blades is caused by the effect of velocity on vortex motion.

5. Conclusion

In order to study the causes of wind turbine blade aerodynamic noise, this paper analyzed the distribution of wind turbine sound field and flow field by means of numerical simulation. Then the vortex theory is used to compare and analyze the distribution law of sound field and flow field, and the main conclusions are as follows:

(1)Through numerical simulation and test measurement, the directivity characteristics of wind turbine aerodynamic noise sound source are analyzed. The directivity characteristics are dipole characteristics and belong to dipole sound source.

(2)The sound source of wind turbine blade aerodynamic noise is mainly distributed in 65%~95% span of the blade. The sound pressure level of the pneumatic noise source changes slightly in the 65%-85% span, but decreases significantly in the 85%-95% span.

(3)The vortex motion caused by fluid motion is the main cause of aerodynamic noise of wind turbine blades. The distribution law of wind turbine blade aerodynamic noise sound pressure level is very consistent with the distribution law of vortex motion.

Acknowledgements

The above study was supported by National Natural Science Foundation of China Project "Research on Dynamic Evolution Mechanism and Active Control of the axis Locus of hydrostatic electric Spindle under Multi-field Coupling" (51875198), Key project of Hunan Provincial Department of Education "Research on the Formation and Evolution Mechanism of oil film Holes in hydrostatic motorized spindle and its Active Control Method" (23A0360), Science and Technology Research Project of Xiangtan Science and Technology Bureau "Research on Active control and Evaluation Technology of Variable Mass unbalanced rotor system of Ultra-High Speed maglev Permanent magnet synchronous motorized spindle" (GX-YB20221004).

References

[1] Liu W Y. A review on wind turbine noise mechanism and de-noising techniques[J]. Renewable Energy, 2017, 108: 311-320.
[2] Powell A. Theory of vortex sound[J]. Journal of the Acoustical Society of America, 1964, 36(1): 177-195.
[3] Howe M S. Theory of vortex sound[M]. New York: Cambridge University Press, 2003.
[4] Howe, M.S. " Contributions to the theory of aerodynamic sound with applications to excess noise jet noise and the theory of the flute." [J]. Fluid. Mech.71, pp. 625-673
[5] Violato D, Moore P, Bryon K, et al. Application of Powell's analogy for the prediction of vortex-pairing sound in a low-Mach number jet based on time-resolved planar and tomographic PIV[C]//16th AIAA/CEAS Aeroacoustics Conference. 2010: 39-59.
[6] Tang S K, Ko N W M. Basic sound generation mechanisms in inviscid vortex interactions at low Mach number [J]. Journal of sound and vibration, 2003, 262(1): 87-115.
[7] Zheng C, Zhou P, Zhong S, et al. Experimental investigation on cylinder noise and its reductions by identifying aerodynamic sound sources in flow fields[J]. Physics of Fluids, 2023, 35(3).
[8] Ouyang H, Tian J, Wu YD, et al, Research on aerodynamic noise of low-speed axial fan based on vortex sound theory[J]. Journal of Engineering Thermophysics. 2009. 30(05): 765-768
[9] Zhang N, Hua X I E, Xing W, et al. Computation of vortical flow and flow induced noise by large eddy simulation with FW-H acoustic analogy and Powell vortex sound theory[J]. Journal of Hydrodynamics, Ser. B, 2016, 28(2): 255-266.
[10] Si Q, Ali A, Tian D, et al. Prediction of hydrodynamic noise in ducted propeller using flow field-acoustic field coupled simulation technique based on novel vortex sound theory[J]. Ocean Engineering, 2023, 272: 113907.
[11] Guo C. Research on coupling mechanism of three-dimensional flow field and induced sound field in centrifugal pump based on Powell vortex sound theory[D]. Shandong University. 2020.
[12] Wang XZ. Physical Hydrodynamics[M]. Beijing: Tsinghua University Press. 2018. 58-93

ISSN 2616-5767 Vol.7, Issue 3: 17-28, DOI: 10.25236/AJETS.2024.070304

[13] Králik J. CFD simulation of air flow over an object with gable roof, revised with Y+ approach[J]. Transactions of the VŠB – Technical University of Ostrava. 2016. DOI: 10.1515/tvsb-2016-0018
[14] Si Q, Ali A, Tian D, et al. Prediction of hydrodynamic noise in ducted propeller using flow field-acoustic field coupled simulation technique based on novel vortex sound theory[J]. Ocean Engineering, 2023, 272: 113907.
[15] Zhang HL. Theoretical Acoustics[M]. Beijing: Higher Education Press. 2017. 7. 245-379
[16] Zhuai GQ, XU J, ZHENG Y, et al. Noise prediction of wind turbines[J]. China Environmental Science. 2012. 32(05): 927-932.
[17] Xu XM. Fundamentals of Acoustics [M]. Beijing: Science Press. 2003. 157-198
[18] Zhou JF. Fundamentals of Fluid Mechanics [M]. Beijing: Chemical Industry Press. 2018. 225-253